J. Anat. (2007) **211**, pp798–809 doi: 10.1111/j.1469-7580.2007.00825.x

Micro-magnetic resonance imaging of avian embryos

Xiaojing Li,[1] Jia Liu,[1] Megan Davey,[2] Suzanne Duce,[1] Neema Jaberi,[2] Gang Liu,[1] Gemma Davidson,[2] Seaneen Tenent,[2] Ruth Mahood,[2] Phoebe Brown,[2] Craig Cunningham,[2] Andrew Bain,[2] Kevin Beattie,[2] Laura McDonald,[2] Katy Schmidt,[2] Matthew Towers,[2] Cheryll Tickle[2] and Sandy Chudek[1]

[1]*Division of Biological Chemistry and Drug Discovery,* [2]*Division of Cell and Developmental Biology, College of Life Sciences, University of Dundee, Dundee, UK*

Abstract

Chick embryos are useful models for probing developmental mechanisms including those involved in organogenesis. In addition to classic embryological manipulations, it is possible to test the function of molecules and genes while the embryo remains within the egg. Here we define conditions for imaging chick embryo anatomy and for visualising living quail embryos. We focus on the developing limb and describe how different tissues can be imaged using micro-magnetic resonance imaging and this information then synthesised, using a three-dimensional visualisation package, into detailed anatomy. We illustrate the potential for micro-magnetic resonance imaging to analyse phenotypic changes following chick limb manipulation. The work with the living quail embryos lays the foundations for using micro-magnetic resonance imaging as an experimental tool to follow the consequences of such manipulations over time.
Key words anatomy; avian; chick; embryo; limb development; using micro-magnetic resonance imaging; magnetic resonance imaging; quail.

Introduction

Chick embryos, because of their manipulability, are very influential models for understanding development and how constituent parts of the body form. There are a number of methods that allow molecular and/or genetic analyses, including local application of defined molecules and transient transgenesis (reviewed by Davey & Tickle, 2007). However, to exploit these advances fully, we also need to optimise the analysis of chick anatomy so that we can appreciate all the phenotypic consequences of these manipulations. Here we define conditions for imaging both fixed and living avian embryos using micro-magnetic resonance imaging (μMRI). We focus on the complex anatomy of the developing chick limb and show that, by analysing the μMRI data with a three-dimensional (3D) visualisation package, it is possible to maximise information about several different tissues in the same limb.

MRI relies on the interaction between the spin of atomic nuclei and strong magnetic fields. In MRI, the magnitude of the strength of these interactions gives data which can be used to build up images. An MRI image is a map of the distribution of hydrogen nuclei, usually from water protons in the tissue. The intensities found in the images may be related to water concentration but are modified by the interaction of the water with the different tissues present in the sample, so that even where the water concentration in different tissues is equal, there is image contrast between these tissues. Final image contrast is highly dependent on the experimental parameters used in the image acquisition and, as will be seen below, they can significantly affect these intensity ratios.

In an MRI experiment, the nuclear spin of hydrogen nuclei is excited into a higher energy level and then energy is dissipated through two mechanisms, longitudinal (T_1) and transverse (T_2) relaxation, both related to local molecular motions. Thus interaction of the water with the tissue affects relaxation rates and experimental acquisition parameters T_R (repetition time) and T_E (echo time) can exploit these varying relaxation rates to influence image intensity and highlight different tissue types (Kuhn, 1990; Callaghan, 1995). In μMRI, as used here, the external magnet and applied magnetic field gradients are considerably stronger than those used in routine whole body MRI, which allows samples to be imaged with a pixel resolution of the order of 10 μm, although this is again dependent on experimental conditions and certain other considerations (see Chudek & Hunter, 1997).

Micro-MRI images can be enhanced by using paramagnetic molecules such as gadolinium as contrast agents. Gadolinium ion is administered chelated within a shell of organic ligands to protect the living organism from the toxicity of free gadolinium ion. The organic shell is designed to allow the interaction between the paramagnetic agent and the water in the tissues of the sample. Gadolinium reduces

Correspondence
Dr Sandy Chudek, Division of Biological Chemistry and Drug Discovery, College of Life Sciences, University of Dundee, Dundee, UK.
E: j.a.chudek@dundee.ac.uk

Accepted for publication *10 September 2007*

the relaxation rates of the water protons in the tissues (Hendrick & Haacke, 1993; Nelson & Runge, 1995).

Micro-MRI has been used to produce several 3D digital atlases of mouse embryos (Smith et al. 1994; Dehain et al. 2001), and μMRI imaging of the anatomy of mouse embryos is being increasingly used to analyse phenotypes following genetic manipulations (Schneider et al. 2003). Surprisingly, however, despite sporadic reports over the last 20 years, μMRI has been relatively rarely applied to chick and other avian embryos [but see, for example, Hogers et al. (2001)]. Recently, an atlas of quail anatomy has been published (Ruffins et al. 2007) and websites containing data covering the later stages of development of avian embryos has been launched (http://atlasserv.caltech.edu/Quail/Start_Quail.html, http://chickscope.beckman.uiuc.edu/) (Bruce et al. 1997). However, the issue of the usefulness of μMRI as a tool to examine experimentally manipulated chick or quail embryos has not been addressed. In addition, as μMRI is non-invasive, it can be applied to living animals. Therefore avian embryos which come conveniently packaged in eggs offer the prospect of using μMRI to follow the development of live embryos of a higher vertebrate and again, although this possibility was recognised a long time ago (Bone et al. 1986, Effmann et al. 1988), it has not been exploited.

In this paper, we have focused particularly on visualising the anatomy of the chick limb using μMRI. The limb is a classic example where studies on chicks have cast light on general developmental principles. The three major sets of cell–cell interactions involved in vertebrate limb development were discovered in chick embryos; furthermore, the activity of defined chemicals that mediate these interactions was also first demonstrated in chicks (reviewed in Niswander, 2003; Tickle, 2004). The read-out of the effects of experimental and genetic manipulations on chick limb development has usually been in terms of the skeleton, which can be readily stained in whole mounts with Alcian Blue and Alizarin Red to show cartilage and bone, respectively. Some studies have investigated the musculature of manipulated limbs in sections (Robson et al. 1994; Duprez et al. 1999), which is very time-consuming, and early muscle development has been visualised using whole mount immunohistochemical staining (Kardon, 1998). One of the main issues is how the pattern of the different tissues in the limb is co-ordinated at both cellular and genetic levels. Here we have used different μMRI protocols and acquisition parameters to differentiate various tissues in the same limb, while taking advantage of the ability to produce 3D digitised images which allow us to visualise precise anatomy.

Materials and methods

Chicken embryos

Fertilised White Leghorn chicken eggs (from H. Stewart, Lincolnshire) were incubated at 37 °C until they had reached the appropriate Hamburger Hamilton (HH) stage (Hamburger & Hamilton, 1951). For examining normal anatomy, the embryos were then removed from the egg and most were fixed in 1–4% paraformaldehyde for least 12 h. Diethylenetriaminepentaacetic acid gadolinium(III) dihydrogen salt hydrate (Omniscan©; GE Healthcare, Slough, UK) a contrast agent used in medical MRI and referred to henceforth as Gd contrast agent, was used to enhance the resolution of images of some samples. For younger embryos, 100 μL Gd contrast agent diluted 50 times in phosphate-buffered saline (PBS) (sometimes with addition of 10% gelatine) was injected with 3 μL fast green into the extra-embryonic blood vessels and left to circulate until the fast green was visible in the wing bud vasculature. The embryos were removed from the egg into PBS and either mounted in Fomblin LC808 (Solvay Solexis, Milan, Italy), a dense fluid totally transparent to MRI (see below), or fixed. For other embryos, the extra-embryonic membranes were torn and 20 μL of neat Gd contrast agent was dropped onto the exposed embryo, which was left for approximately 1 h, then removed from the egg, and fixed.

Quail embryos

Fertilised quail eggs were obtained from the Roslin Institute and incubated. Embryos were removed from the eggs and fixed as above. Staging of quail embryos is described in Graham & Meier (1975). Quail eggs can be accommodated in a 30 mm MRI resonator (see below) and thus live embryos could be imaged while still inside the egg. A window was made in the eggshell and this was then re-sealed with clear sticky tape until the embryo reached the desired stage. Then 40 μL of the Gd contrast agent (as supplied, diluted 10 times with PBS) was either dropped onto the embryo in the egg or injected into the abdomen of the embryo or into an extra-embryonic artery before imaging.

Mounting embryos for imaging

The majority of the specimens described here were mounted in Fomblin. Embryos were placed in a tube sufficiently wide enough to ensure the sample did not touch the sides; flexible plastic tubing was used to hold the sample in position and Fomblin was added following methods described for mouse embryos (Smith, 2000). The Fomblin sealed the sample and allowed it to float so that it was securely held by the tubing.

Some specimens were embedded in 1% agar gel dissolved in deionised water. The agar was left to cool down and, if not otherwise mentioned in the text, the Gd contrast agent (0.5 mmol mL^{-1}) was added at 60 μL mL^{-1} and mixed gently. The solution was poured into an MRI tube of suitable size to form a platform for the specimen to sit on. Embryos were then placed on the platform and the tube

was topped up with agar until the embryo was completely covered.

Quail eggs were placed directly into the imaging probe fitted with a 30 mm resonator and stabilised using PTFE tape.

Skeletal staining with Alcian Blue–Alizarin Red

Embryos were fixed in ethanol for 1 week, post-fixed in acetone for 1 week, stained in 0.015% Alcian Blue, 0.005% Alizarin Red in 70% ethanol for 1 week, cleared in 20% glycerol, 0.1% KOH for 3 days and then put through successive washes of glycerol up to 100% glycerol. To visualise the histology, a few whole mounts were dehydrated through a series of ethanol, cleared, then embedded in wax, sectioned and examined using standard optical microscopy techniques.

Chick limb bud manipulation

AG1X-2 beads were soaked in 5 mg mL^{-1} all trans-retinoic acid (Sigma, St Louis, MO, USA) and implanted at the anterior margin of stage 20 chick wing buds as described by Tickle et al. (1985). The embryos were then re-incubated for a further 9 days. The operated and contralateral control wings were then fixed in 4% paraformaldehyde.

Micro-MRI

Data for images were accumulated on a Bruker AVANCE FT NMR spectrometer (Rheinstetten, Germany) with a 7.1T wide bore vertical magnet resonating at 300 MHz for ^{1}H. The spectrometer was fitted with a Bruker Microimaging accessory and probe equipped with birdcage resonators with internal diameters ranging from 10 to 30 mm in diameter. Generally, samples were imaged using a resonator slightly larger than the sample diameter to minimise artefacts; a coil into which the sample fits neatly will give an optimum signal to noise ratio, but too close a proximity of the transmitter/receiver coil to the sample may cause distortions in the final image and where possible these were avoided. Pulse sequences were from the Bruker Paravision® library. The imaging experimental parameters are noted in both text and figure legends. For all samples, the probe was tuned and the magnet shimmed before data acquisition, two acquisition sequences were collected and averaged to improve signal-to-noise ratio and to remove artefacts. Total acquisition times varied depending on both T_E and matrix size, ranging from around 4 h for imaging eggs containing live embryos up to 16 h for fixed specimens acquired at high resolution. All acquisitions were made at 19 °C. At this temperature the heart beat of living embryos is massively reduced and it is well known that early embryos can withstand large, temporary, falls in temperature (e.g. New, 1966). Imaging data were Fourier transformed, and then transferred to a PC for final visualisation using AMIRA® imaging software (Mercury Computer Systems, Inc., TGS unit, Whyteleafe, UK). Most images described here were, unless specified as gradient echo in the text, acquired using a 3D spin-echo sequence. The various T_Rs and T_Es are given in the text. Data (unless noted in the text) were collected into $128 \times 128 \times 128$ matrices and transformed into images of the same dimensions. Fields-of-view (the volume scanned) were set to encompass the whole sample and these, in conjunction with the matrix size, determined the final voxel size and spatial resolution. Individual voxel sizes are reported in the figure legends. To ensure reproducibility a minimum of three samples were imaged for each stage and tissue type shown.

The AMIRA software allowed 3D images to be viewed from any angle and construction of pseudo 3D surface rendered images. More importantly, datasets, acquired using different experimental parameters, could be overlaid and superimposed to build up the musculoskeletal anatomy (see below).

Results

Imaging chick embryo anatomy with MRI

We first investigated empirically the parameters for imaging fixed chick embryos at 9–10 days of development (approximately stages 35–36) in tubes containing Fomblin using the spin echo imaging pulse sequence. Figure 1 shows the effects of varying T_R and T_E on images of chick embryos and their internal organs. The upper panels show representative longitudinal sections through a series of whole embryos, anterior to top, posterior to bottom. Figure 1(A) shows a 9-day-old embryo imaged using T_R/T_E = 50/20 ms. Although we can make out the overall structure of the embryo, e.g. head, trunk and tail, we could not distinguish any internal details. When the T_E was reduced to 2.5 ms (Fig. 1B), image quality improved and the vitreous chamber of the eye and various cavities of the brain, for example, could be distinguished. Increasing the T_R to 500 ms improved the image contrast still further (Fig. 1C) and, in addition, organs such as the heart could be clearly seen. In Fig. 1(D), a gradient echo imaging pulse sequence was used but fewer details of the internal structures of the 9-day embryo appeared to be revealed. Therefore the best images of fixed whole chick embryos of this age were obtained using spin echo acquisitions with T_R/T_E = 500/2.5 ms (as shown in Fig. 1C).

The central panels of Fig. 1 show effects of altering T_E and T_R on spin echo images of internal organs of the excised trunk of a stage 36 (10-day-old) chick embryo (Fig. 1E–H). Panels (E) and (F) of Fig. 1 show longitudinal and transverse sections respectively, imaged with similar parameters to Fig. 1(C) T_R/T_E = 200/6.3 ms, which reveal details of internal organs including heart, vertebrae,

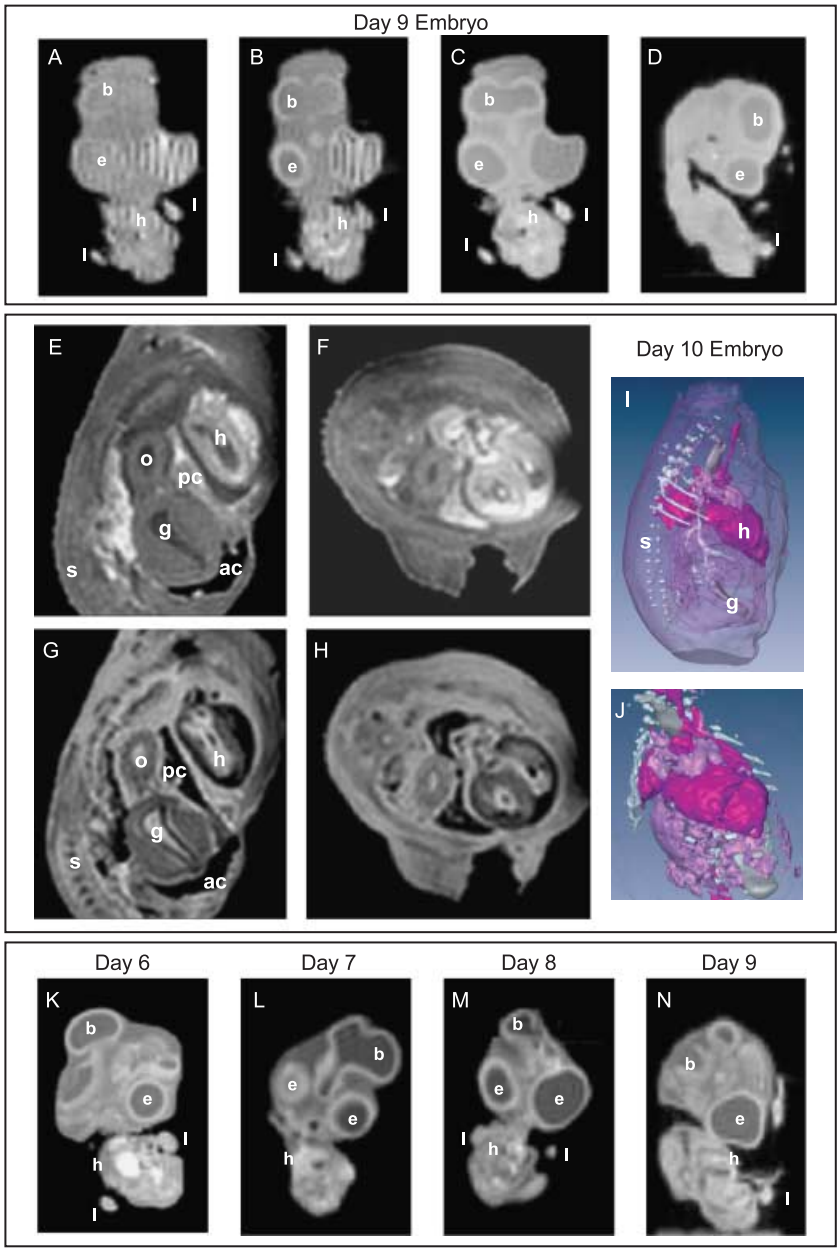

Fig. 1 μMRI images of chick embryos. (A–D) Day 9 embryos, (E–J) Day 10 embryo, (K) Day 6 embryo, (L) Day 7 embryo, (M) Day 8 embryo, (N) Day 9 embryo. The MRI experimental parameters varied: (A–C) spin echo images, (A) T_R/T_E = 50/20 ms; (B) T_R/T_E = 50/2.5 ms; (C) T_R/T_E = 500/2.5 ms. (D) gradient-echo image T_R/T_E = 50/2.5 ms. (E–M) spin echo images, (E and F) longitudinal and transverse slices, respectively, from a 3D dataset with T_R/T_E = 200/6.3 ms. (G and H, respectively) The same slices as (E and F) but with T_R/T_E = 2000/35 ms. (I and J) 3D surface rendering from 3D dataset (T_R/T_E = 200/6.3 ms), manually extracting anatomy of interest using AMIRA. (K–N) T_R/T_E = 500/2.5 ms. All matrix sizes are 128 × 128 × 128. Field of view and voxel dimensions: (A–D) 4.0 × 4.0 × 4.0 mm; 32 × 32 × 32 μm, (E–H) 10 × 10 × 10 mm; 80 × 80 × 80 μm, (K) 2.8 × 2.8 × 2.8 mm; 22 × 22 × 22 μm, (L) 3.0 × 3.0 × 3.0 mm; 24 × 24 × 24 μm, (M and N) 5.0 × 5.0 × 5.0 mm; 40 × 40 × 40 μm. s, spine; e, eye; h, heart; b, brain; l, limb; g, gizzard; o, oesophagus; ac, abdominal cavity; pc, pleural cavity.

gizzard and oesophagus. Panels (G) and (H) of Fig. 1 show the same specimen, again sectioned longitudinally and transversely, but this time imaged with a greatly increased T_R and T_E, T_R/T_E = 2000/35 ms. Altering these parameters has profound effects on the appearance of the embryo. For example, in Fig. 1(E and F), the pleural cavity and the inside of the gizzard appear dark whereas in Fig. 1(G and H) the cavities are light. In addition, more importantly, further anatomical details can be seen, with, for example, vertebrae being clearly distinguished in the spine in Fig. 1(G) but not in (E). Panels (I) and (J) of Fig. 1 show 3D reconstructions from the dataset used in (G) and (H), highlighting parts of the vertebrae and associated ribs and the heart. The full dataset used to reconstruct these images is shown in Supplementary material, Video clip S1(a) and an animation of the reconstruction can be seen in Supplementary material Video clip S1(b). These extended parameters furnish more detailed anatomy than the shorter parameters but require an acquisition time 10 times greater (here the acquisition time was 1 h 49 m when T_R was 200 ms and 18 h 12 m when the T_R was 2000 ms).

We then investigated whether we could apply these parameters to imaging younger chick embryos. Panels (K–N) of Fig. 1 show representative longitudinal sections through a series of fixed chick embryos aged between days 6 and 9 (approximately HH stages 28–35) imaged with T_R/T_E = 500/2.5 ms. Even in the youngest embryo (Fig. 1K) a considerable amount of anatomical detail can

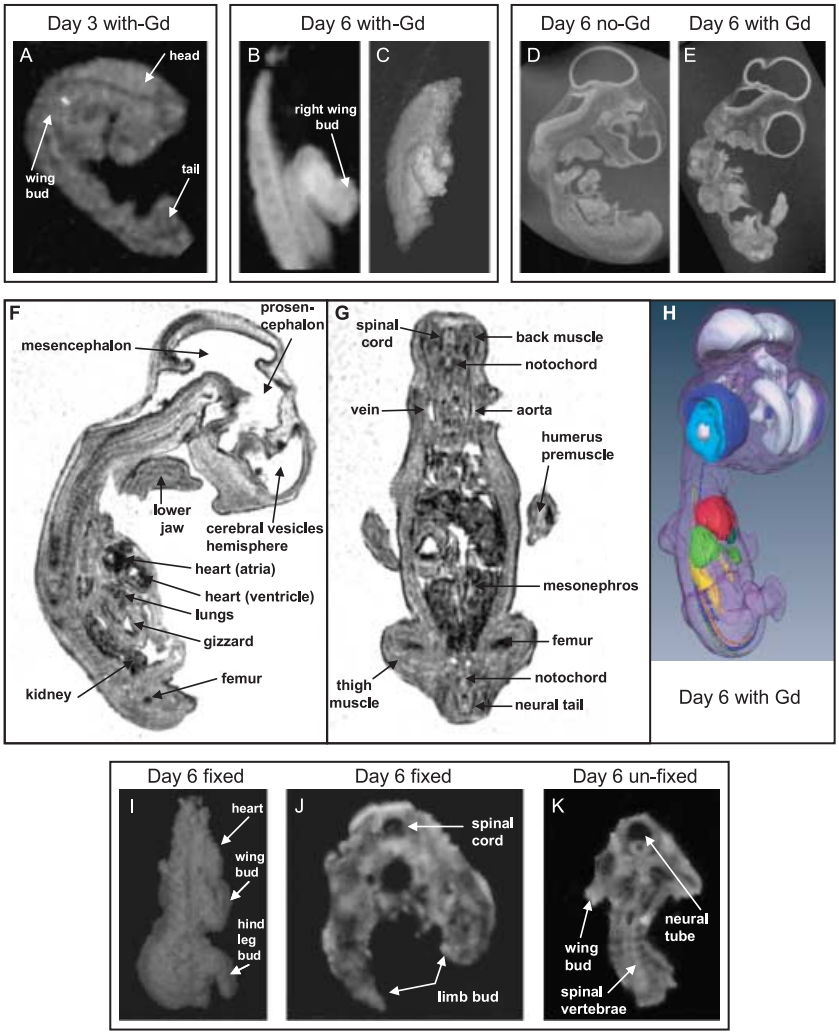

Fig. 2 3D μMRI spin echo images of chick embryos. (A–C) Embryos injected with gadolinium (Gd) contrast agent before harvesting. (A) Day 3 embryo. (B) Day 6 embryo. (C) Surface rendering of Day 6 embryo. (D) Day 6 embryo (fixed without addition of Gd contrast agent and embedded in agar). (E) Day 6 embryo (20 μL of Gd contrast agent was dropped onto embryo while in the egg, fixed after 1 h and embedded in agar). (F–H) Day 6 embryo (Gd contrast agent applied in ovo, fixed after 1 h and embedded in agar containing contrast agent), (H) 3D surface rendering of selected anatomy. (I–K) Injected with gelatine containing Gd contrast agent. (I) Fixed Day 6 embryo. (J) Fixed Day 6 embryo. (K) Unfixed Day 6 embryo. MRI experimental parameters varied: (A) T_R/T_E = 1000/35 ms, (B and C) T_R/T_E = 400/2.6 ms, (D–H) T_R/T_E = 300/10 ms, (I and J) T_R/T_E = 1000/55 ms, (K), T_R/T_E = 400/2.4 ms. Matrix sizes: (A–C) and (I–K) 128 × 128 × 128, (D and E) 256 × 256 × 256, (F–H) 512 × 512 × 512. Field of view and voxel dimensions: (A) 2.5 × 2.5 × 2.5 mm; 20 × 20 × 20 μm, (B–C) 24 × 24 × 24 μm, (D and E) 10.0 × 10.0 × 10.0 mm; 40 × 40 × 40 μm, (F–H) 10.0 × 10.0 × 10.0 mm; 20 × 20 × 20 μm, (I–K) 2.5 × 2.5 × 2.5 mm; 20 × 20 × 20 μm.

be seen in both head and trunk, including eye and brain cavities and the outline of the heart.

Use of gadolinium contrast agents in imaging young chick embryos

The anatomy described above was obtained using fixed embryos but it has been reported that μMRI imaging of mouse embryos is significantly improved by the use of gadolinium contrast agents (Schneider et al. 2003). Therefore we investigated the effects of contrast agents on imaging chick anatomy and, in addition, because in the long term we wish to use μMRI to follow organogenesis in the embryo, we also investigated whether contrast agents could improve the image contrast of younger embryos including unfixed specimens.

We first investigated various methods of applying the Gd contrast agent to chick embryos and monitored effects on the images obtained. We injected Gd contrast agents into the vascular system of Day 3 and Day 6 (stage 20 and stage 28) chicken embryos before fixing them and imaging them using similar MRI experimental parameters as those outlined above (Fig. 2A–C). Gross features of a stage 20 chick embryo, including head and heart, could be observed using spin echo with a T_R/T_E = 1000/35 ms (Fig. 2A). Only part of the trunk was imaged for a stage 28 embryo (spin echo T_R/T_E = 400/2.6 ms) and both sagittal sections and surface rendering showed the outline of the developing wing very clearly (Fig. 2B,C).

In the next series of experiments we tested various methods of applying Gd contrast agent and its effect on the quality of the images obtained of stage 28 chick embryos. Figure 2(E) shows a section through an embryo in which 20 μL of the Gd contrast agent was dropped on to it through a window in the shell while it was still alive and in the egg. The embryo was then fixed 1 h later and imaged using T_R/T_E = 300/10 ms (compare with Fig. 2D embryo fixed without addition of contrast agent). The application of the Gd contrast agent resulted in improved resolution of anatomical detail, particularly with respect to internal organs. Whilst the T_Rs of the latter acquisitions were shorter than that used in Fig. 2A, it was found that

this reduction led to very little change in contrast or decrease in overall image intensity. The effect of varying T_E can be seen in the variation of image intensity and contrast in the various images. We also took some of these embryos to which contrast agent had been applied *in ovo* and then had been fixed after 1 h and embedded them in agar containing the Gd contrast agent. Figure 2(F,G) shows representative sections of one of these embryos (Supplementary material Video clip S2a,b shows the complete dataset viewed in the same orientation as that shown in Fig. 2F and G, respectively). Embedding in agar significantly improved the image contrast and emphasized internal structures thus revealing details of the structure of the heart, brain and spinal cord, etc. Figure 2(H) shows a surface reconstruction of different organs including the brain cavity, spinal cord and heart.

In the third series of experiments, we injected gelatine containing Gd contrast agent into the vascular system and then compared images of fixed and unfixed Day 6 (stage 25) embryos, thus taking a step nearer imaging live embryos. One chicken embryo was fixed for 24 h (Fig. 2I,J) before imaging and the other was directly imaged without fixing (Fig. 2K); panel (I) shows a surface reconstruction of the fixed embryo while panels (J) and (K) show sections of the fixed and unfixed embryos, respectively. To obtain the optimal images at these stages, the fixed embryos were imaged using spin echo T_R/T_E = 1000/55 ms similar to the fixed stage 20 embryos, whereas the unfixed embryos were imaged using spin echo T_R/T_E = 400/2.4 ms. In the surface reconstruction, one can make out the trunk and limbs. The slices reveal details of the spinal cord; both notochord and neural tube are clearly visible in the unfixed specimen in addition to developing vertebrae (Fig. 2K).

Taking all these results together the best resolved anatomical images were obtained when the Gd contrast agent was dropped on to the live embryo *in ovo* and the fixed embryo then embedded in agar containing the Gd contrast agent. In addition, injection of the Gd contrast agent into an embryo allowed well resolved images to be obtained from unfixed material and therefore suggested conditions that would allow imaging of living avian embryos at early stages of development.

Micro-MRI of living quail embryos

As the bore of the MRI magnet is too narrow to accommodate chicken eggs, we therefore turned to quails, which have smaller eggs and slightly smaller embryos. First we imaged a series of fixed quail embryos from 5 to 8 days of development. Using the same parameters as those employed in collecting images shown in Figures 1 and 2 (T_R/T_E = 500/2.5 ms), we obtained images which showed considerable anatomical detail. Figure 3(A–D) shows a longitudinal slice through a quail embryo at each of the different stages of development. These images reveal details of internal anatomy, including regions of the brain, heart, limb, intestine and spine. In the 8-day quail embryo, the lens of the eye is clearly visible. The images are comparable to those of chick embryos at the same age and the older embryos generally show more structure.

We then injected the Gd contrast agent into 7-day quail embryos and imaged them using MRI (with spin echo T_R/T_E = 500/2.5 ms) either after removal from the egg and fixation (Fig. 3E) or inside the egg (Fig. 3G–M) (compare Fig. 3G and I, J and K with Fig. 3C, a quail embryo of the same age fixed but not previously exposed to contrast agents) and a quail embryo stained for bone and cartilage (Fig. 3F). The injection of Gd contrast agent into the abdomen of the embryo increases the brightness of the internal structures after fixation (compare Fig. 3E with 3C). More significantly, the injection of Gd contrast agent allowed visualisation of gross features of the live quail embryo in the egg including the head, brain, spinal cord and eye (Fig. 3G,H) (Supplementary material Video clip S3 shows an animation of this 3D reconstruction). A second live quail embryo was imaged after injection of contrast agent into the egg near the head (Fig. 3I–M). This revealed a wealth of detail in both head and body (see slices Fig. 3I–K and M and reconstruction Fig. 3L). We also inspected the image of the limbs in some detail (Fig. 3M leg outlined). We could detect a region of different intensity internally but we could not make out whether this represented skeletal structures. A few experiments were carried out in which live 7-day quail embryos were imaged inside the egg without the addition of contrast agent. At this stage of development, differentiation between the embryo and other egg contents was poor (data not shown).

Chick limb anatomy

Skeleton

We then focused on imaging the skeletal anatomy of fixed chick embryonic limbs (3% paraformaldehyde being found to be better than 1%). MRI allowed good visualisation of the cartilaginous limb skeleton using a spin echo imaging pulse sequence and T_R/T_E = 1000/5 ms. Figure 4(A–D) shows maximum intensity projection MRI images of wings from chick embryos at between Day 10 and 13 of development (stages 36–39). By 10 days (stage 36), all the main skeletal elements of the wing, humerus, radius, ulna and digit metacarpals have been laid down in cartilage. These are clearly defined by MRI and appear bright white. Most of the skeletal elements in the digits can also be seen, for example, the two phalanges in digit three (Fig. 4A). Humerus, radius and ulna are thinner in the central regions than at the ends. This thinning of the cartilaginous skeletal elements in the central regions is more marked at later stages. In 11-day wings, the skeletal elements taper

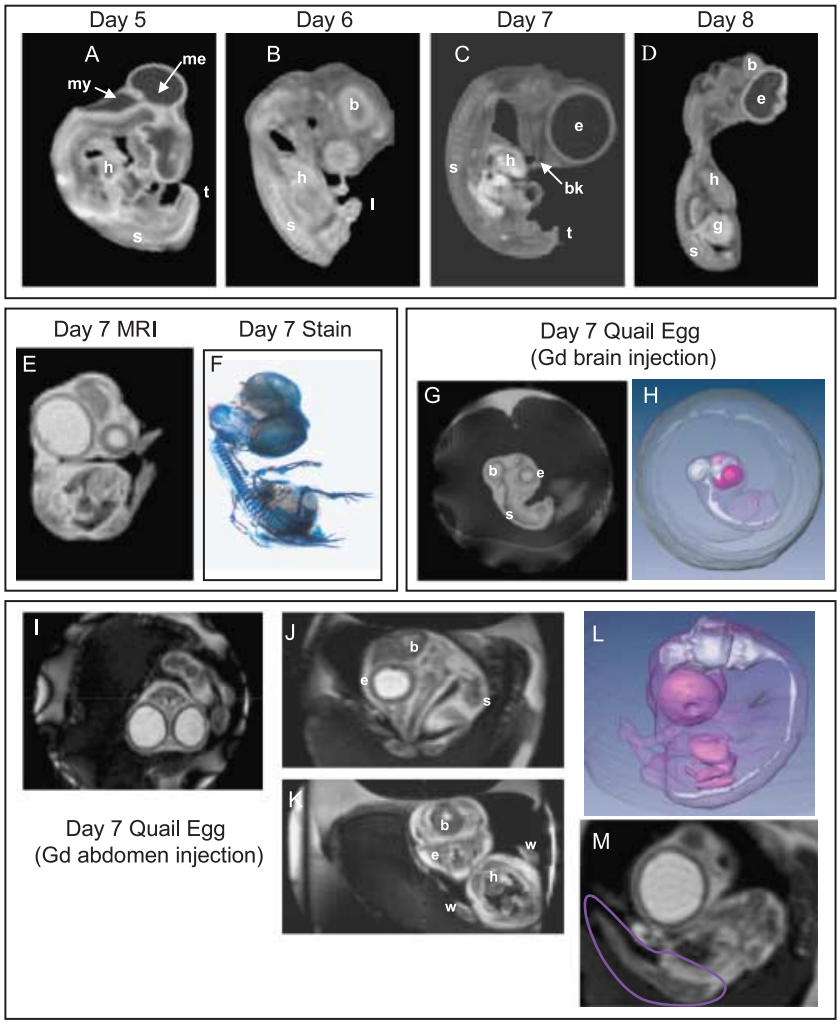

Fig. 3 3D μMRI spin echo images of quail embryos (T_R/T_E = 500/2.5 ms). (A) Day 5 quail embryo. (B) Day 6 quail embryo. (C) Day 7 quail embryo. (D) Day 8 quail embryo. (E) Day 7 quail embryo injected in the abdomen with the Gd contrast agent while in the egg, then harvested and fixed. (F) Day 7 quail embryo stained for bone and cartilage. (G and H) Living Day 7 quail embryo in its egg, after injection with contrast agent in the abdomen, (H) 3D surface rendering of regions of interest using AMIRA software. (I–O) Living Day 7 quail embryo in its egg, after injection with the Gd contrast agent in the abdomen. (J and K) Orthogonal slices. (L) 3D surface rendering of regions of interest using AMIRA software. (M) Expansion of the right hind leg of same embryo highlighting internal structure . All matrix sizes are 128 × 128 × 128. Fields of view and voxel dimensions: (A and B) 2.5 × 2.5 × 2.5 mm; 20 × 20 × 20 μm, (C–E) 3.0 × 3.0 × 3.0 mm; 24 × 24 × 24 μm, (G–N) 30.0 × 30.0 × 30.0 mm; 240 × 240 × 240 μm. s, spine; e, eye; h, heart; b, brain; my, myelocoele; me, mesencephalon; bk, beak; lv, liver; l, limb; g, gizzard; t, tail.

towards the centre and a clear gap between the two tapering ends of the cartilage elements can be seen (Fig. 4B). This gap is even greater in 12- and 13-day wings (Fig. 4C,D). In these later wings, a gap can also be clearly seen in the central region of the metacarpal of digit 3.

Alongside the MRI images are shown whole mounts of chick wings at the same stages (Fig. 4E–H) stained with Alcian Blue and Alizarin Red to show the skeleton (blue being cartilage; red, bone). By 10 days (stage 36) ossification centres have developed in humerus, radius and ulna and the metacarpals of digits 3 and 4, as described in Holder (1978), and these form bone collars. Comparison of the MRI and stained limb skeletons show that the white images of bone produced by MRI are of cartilaginous tissue whereas the mineralised bone is MRI invisible. In the whole mounts of the stained specimens, the bone collar gives rise to a sharp boundary between cartilage and bone and covers the tapering ends of the cartilage, in the central region, as can be seen in a longitudinal wax section of a Day 13 wing (Fig. 4M). Figure 4(I) shows an MRI section through the wing of a Day 14 embryo acquired using the same parameters as in Fig. 4(A–D). Figure 4(K) is an identical MRI slice through the same limb but with the T_E increased to 40 ms; there is a marked difference from the image in Figure 4(I), acquired with a very short T_E, 5 ms, where the signal from the mineralised bone tissue can be seen as the brightest region of the image. These datasets allow two maximum intensity projections to be produced; one showing cartilage (Fig. 4J) and the other, mineralised tissue (Fig. 4L).

Use of the AMIRA software enables the two datasets from Fig. 4(I and K) to be merged and the deposition of the mineralised bone in conjunction with the loss of cartilaginous tissue can then be visualised simultaneously in the same dataset. Figure 4(N) shows a reconstruction of the cartilaginous tissue in a Day 10 chick wing; it clearly shows the distal end of the humerus, radius and ulna, the metacarpals of the three digits and the two distal phalanges in digit 3. In the merged image, an enlargement of the ulna region (Fig. 4O) indicates that a small amount of mineralised tissue (purple) is observable at this stage, mainly around the mid-shaft region. Figure 4(P,Q and R,S) shows the changes seen on Days 12 and 14, respectively, and the thinning and

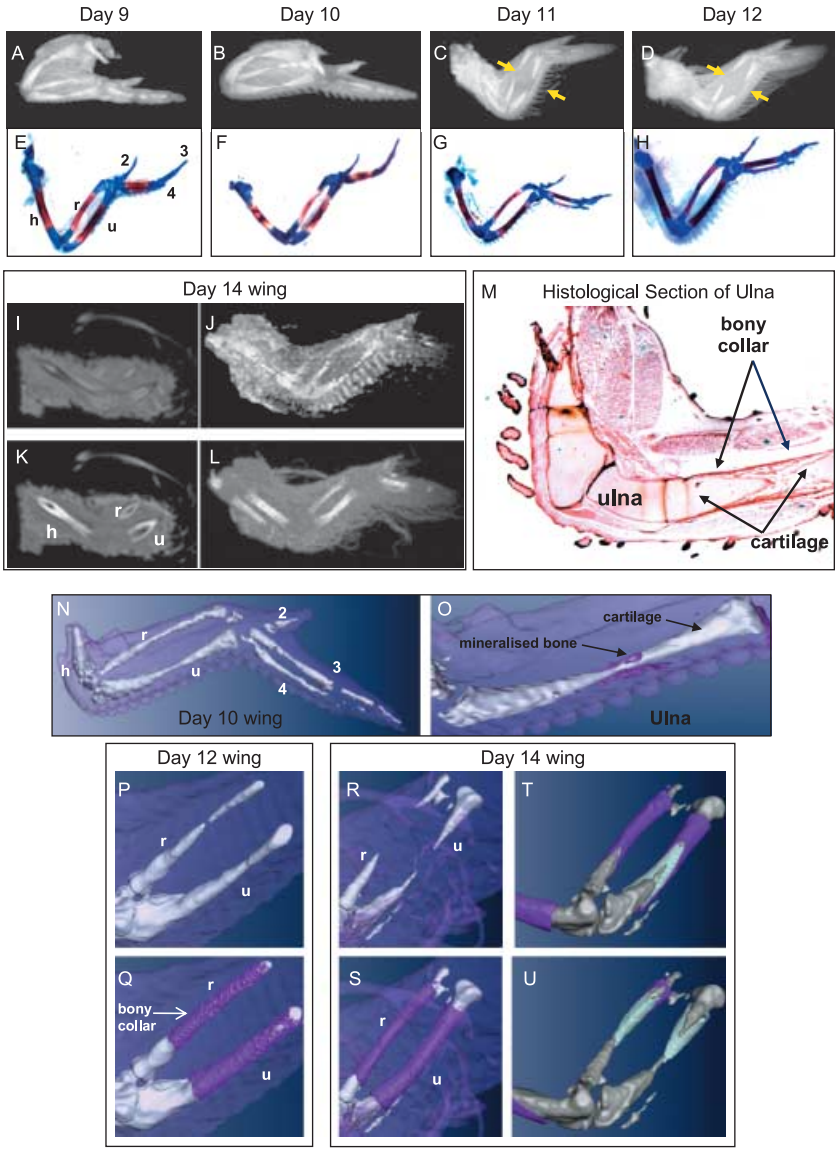

Fig. 4 3D μMRI spin echo images of excised chick embryo wings. (A–D) Maximum intensity projection images of chick wing (T_R/T_E = 1000/5 ms): (A) Day 9 wing, (B) Day 10 wing, (C) Day 11 wing, (D) Day 12 wing. Arrows indicate gap between tapering elements in radius and ulna. (E–H) Stained embryo wings: (E) Day 9, (F) Day 10, (G) Day 11, (H) Day 12. (I–L) Images of Day 14 embryo wing: (I and K) 2D slice, (J and L) maximum intensity projection images. (M) Stained histological section illustrating relationship between cartilaginous tissue and mineralised bony collar. (N–U) 3D composite images of chick embryo wings, surface rendering of skin (shown semi-transparent), cartilaginous tissue (white) and mineralised bony collar (purple) using AMIRA software. (N and O) Day 10 wing; (N) displays cartilaginous tissue and (O) visualises mineralising bone in ulna. (P and Q) Day 12 wing displaying cartilaginous tissue and mineralised bone. (R–U) Day 14 wing displaying cartilaginous tissue and mineralised bone. Mineralised bony collar is digitally removed in (T and U) using AMIRA software. MRI parameters varied: (I and J) T_R/T_E = 1000/5 ms images, (K and L) T_R/T_E = 1000/40 ms images. All matrix sizes are 128 × 128 × 128. Fields of view and voxel dimensions: (A and B) 20.0 × 20.0 × 20.0 mm; 160 × 160 × 160 μm, (C and D) 24.0 × 24.0 × 24.0 mm; 190 × 190 × 190 μm, (I and J) 30.0 × 30.0 × 30.0 mm; 240 × 240 × 240 μm. h, humerus; u, ulna; r, radius; digits 2, 3, 4.

loss of cartilage (Fig. 4P,R) and build up of mineralised bone (Q,S). In Fig. 4(S) the bone collar is seen encasing the cartilaginous rudiment and the cartilaginous epiphyses are visible sticking out at each end. Using AMIRA visualising software, one tissue can be sequentially stripped from the other. This is illustrated in Fig. 4(T,U) and reveals the relationship between the collar of bone and underlying cartilage rudiment as was previously demonstrated by the wax sections. As MRI is a non-destructive technique, however, these MRI images were obtained from an intact specimen (Supplementary material Video clip S4a,b shows more detailed views of the 10- and 14-day wings).

Muscle

Although skeletal elements can be readily identified in chick embryo wings using a spin-echo sequence, distinguishing muscles was more difficult and gradient echo imaging with a very long T_E (40 ms) proved to be a much better method for visualising muscle. Here we focus on chick legs rather than wings, using a series of embryos at different stages of development. Details of the soft tissue become progressively more defined in 12-, 14- and 18-day legs (stages 36–44; Fig. 5A,B and C, respectively. By 14 days, not only are the outlines of individual muscles well defined, allowing identification of individual muscles, but also muscle striations can be seen. In addition, some internal structure can be made out within the bones.

Figure 5(D) shows a longitudinal slice from a 3D dataset acquired from the 18-day leg. From this dataset the AMIRA software allowed a surface rendered image of individual muscle groups to be constructed (Fig. 5E and Supplementary material Video clip S5). For ease of viewing, only four muscles are shown; these are two of the flexor perforatus

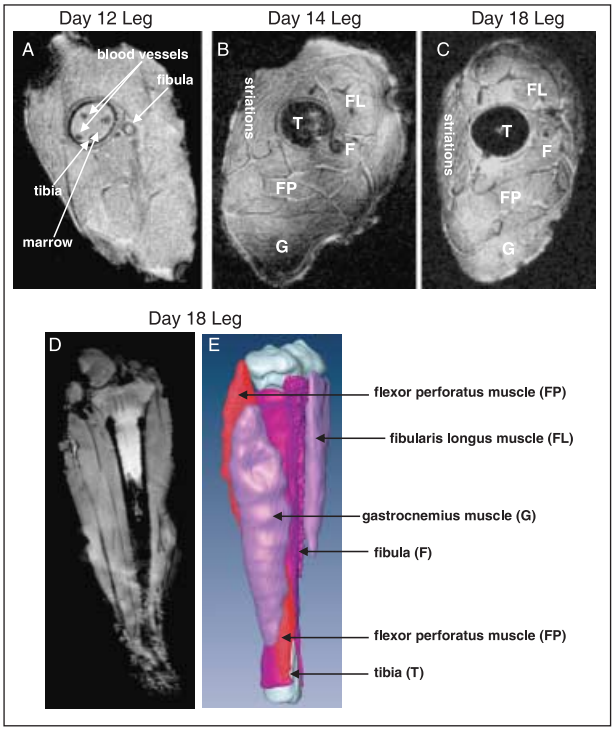

Fig. 5 μMRI gradient-echo images of chick embryo legs. (A) Day 12 leg. (B) Day 14 leg. (C) Day 18 leg. (D) Longitudinal slice from a 3D dataset of Day 18 leg. (E) 3D surface rendering of bones and individual muscles using AMIRA software. T_R/T_E = 1000/40 ms. All matrix sizes are 128 × 128 × 128. Field of view and voxel dimensions are 25.0 × 25.0 × 25.0 mm; 200 × 200 × 200 μm.

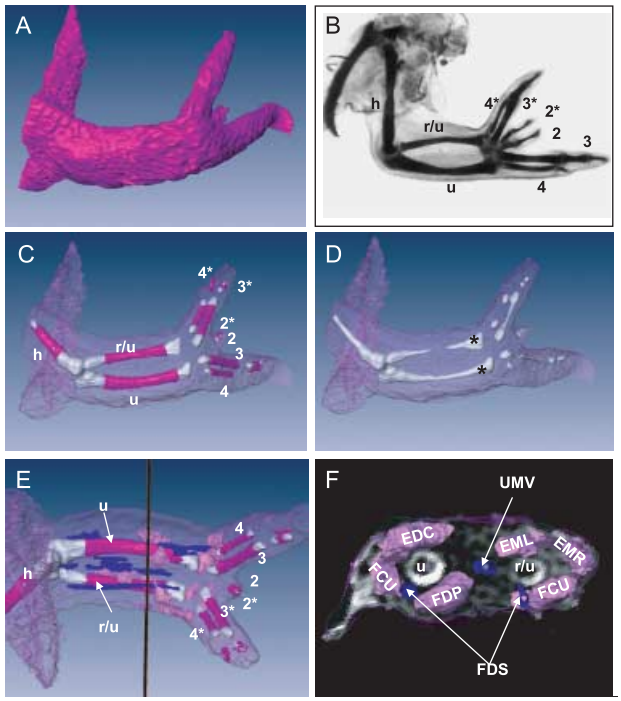

Fig. 6 μMRI gradient-echo images of a Day 13, 432234 experimentally manipulated chick wing. (A) Surface reconstruction of the manipulated wing. (B) Photograph of a stained 10-day wing manipulated in the same manner as that used for μMRI. (C and D) Skeletal elements of the wing, displaying cartilaginous and mineralised tissue (C) and cartilaginous tissue only (D). Note symmetry of the distal epiphyses in the forearm (*). (E) Full reconstruction of the wing showing the position of the slice through the forearm element proximal to the wrist visualised in (F) with 3D surface rendered representations of the muscles and tendons observed in that region superimposed. Images created using data acquired from spin echo, T_R/T_E = 300/40 ms and T_R/T_E = 300/10 ms, and gradient echo, T_R/T_E = 500/40 ms, acquisitions. Matrix size, 256 × 256 × 256. Field of view and voxel dimensions are 12.0 × 12.0 × 12.0 mm; 50 × 50 × 50 μm.

muscles, the fibularis longus muscle and the gastrocnemius muscle. Both the tibia, with cartilaginous and mineralised tissue, and the fibula can be seen.

Analysis of an experimentally manipulated chick wing

Application of retinoic acid to the anterior margin of an early chick wing bud leads to digit duplications in which up to six digits can develop in a mirror image symmetrical pattern, e.g. 432234 (Tickle et al. 1985; Fig 6B). One of such duplicated wings was analysed using μMRI. Three μMRI acquisitions of a Day 13 duplicated wing were performed; two spin-echo acquisitions at low and high T_E and a gradient echo acquisition at long T_E. The data from these were analysed and compared using AMIRA software to generate the images shown in Fig. 6. Figure 6(A) shows a surface view of the wing where a typical 432234 digit pattern can be seen. This 432234 pattern is more apparent in images showing the skeletal elements of the wing (Fig. 6C,D) in which phalanges from all six digits can be seen. Figure 6(C) visualises both the cartilaginous and mineralised bone tissue. In Fig. 6(D) the mineralised tissue has been stripped away, showing details of underlying cartilaginous tissue which tapers towards the central region of the forearm. Furthermore, Fig. 6(D) shows quite clearly that while the morphology of the proximal epiphyseal regions of the cartilage elements in the forearm resembles that seen in normal wings (compare Fig. 6D with Fig. 4R), in contrast, the morphology of the distal epiphyseal regions is symmetrical. The distal epiphyseal region of the anterior element is much broadened and resembles that of the posterior ulna element. This suggests that the radius becomes transformed into an ulna distally.

The presence of muscles can also be detected in the images. Figure 6(F) shows a slice through the forearm element proximal to the wrist (as marked in Fig. 6E) with the muscles in that region superimposed. Several muscles can be identified. Two large muscles are seen ventrally, one underlying each of the skeletal elements and likely representing the normally posteriorly positioned muscles flexor digitorum profundus (FDP) and flexor carpi ulnaris (FCU). In the dorsal region, the muscle pattern appears

more normal, with extensor digitorum communis (EDC) associated with the ulna, and extensor medius ongus (EML) and extensor metacarpi radialis (EMR) with the anterior radius/ulna element. In addition, the flexor digitorum superficialis (FDS) tendon is duplicated ventrally, and the ulnimetacarpalis ventralis (UMV) tendon runs centrally.

Animations of the dataset used to construct these figures, and a reconstruction showing the various elements, can be seen in Supplementary material Video clip S6(a,b).

Table 1 Parameters used to highlight different tissue types

Tissue type	Acquisition sequence	Age	T_E (ms)	T_R (ms)
Whole embryo	Spin echo	Day 5–9	2.5	500
Trunk	Spin echo	Day 10	35	2000
Mineralised bone	Spin echo	Day 9–14	40	1000
Cartilaginous bone	Spin echo	Day 9–14	5	1000
Muscle	Gradient echo	Day 12–18	40	1000
Egg	Spin echo	Day 7	2.5	500

Discussion

We have optimised experimentally the parameters for imaging chick embryos with μMRI over a wide range of developmental stages from early organogenesis. This complements the recent μMRI atlas of quail embryos created by Ruffins et al. (2007) and extends it by including data from both younger and older embryos. Other novel features of our study include visualisation of live embryos and the detailed analysis of the musculoskeletal system of the chick wing and leg.

The majority of the chick embryo images shown here are spin echo pulse sequence images because comparison of spin echo and gradient echo images of whole fixed embryos showed that the gradient echo image exhibited the least anatomical information (see Fig. 1D). Selection of different T_R and T_Es allowed specific regions of the embryo to be highlighted in the spin echo images. Thus for example, in Fig. 1(E,F), in an image of the chick abdomen acquired using a 3D spin echo sequence with T_R/T_E = 200/6.3 ms, the internal cavity of the heart and gizzard is grey whereas with T_R/T_E = 2000/35 ms (Fig. 1G,H), the same regions are white. This change in image contrast is probably due to the T_2 relaxation time of the protons in the cavity being longer than those in the surrounding tissue. The T_2 of the water protons is highly dependent on local molecular motion and in tissues where this is restricted (for example in regions of small, tightly packed cells) T_2 will be shorter. As T_E is increased, image intensity falls off at a rate approximately inversely proportional to the T_2. Image intensities in short T_E and long T_R images approximate to relative proton densities (the amount of water present). In long T_E images, the relative intensities are weighted by the T_2 of the water protons, thus, as might be expected, the behaviour of the MRI image suggests that associated water moves more freely in the cavities than in the surrounding tissues and therefore the relative grey levels are exchanged. Table 1 gives an indication of the optimum parameters we used to image different tissues.

The best anatomical detail in fixed chick embryo images was obtained using the technique previously described for mouse embryos (Schneider et al. 2003). Six-day-old chick embryos were soaked in fixative containing the Gd contrast agent and then mounted in agar containing Gd contrast agent and left for at least 3 days before imaging. This allowed the Gd contrast agent to perfuse the sample and selectively collect in the organs, producing good anatomical image contrast (Fig. 2F,G). Although μMRI cannot achieve the image resolution of optical microscopy, our use of a spin echo imaging protocol has allowed the visualisation of most aspects of the gross anatomy albeit not all of the detail seen in histological sections in the chick atlas (Bellairs & Osmond, 2005). Our preliminary attempts to image 3-day chick embryos were not so successful, although it seems likely that contrast agents will help in visualising early stages in chick development.

MRI is a non-invasive, non-destructive technique and therefore there is the prospect of being able to use μMRI to follow development of living embryos over time. Here we have described parameters for producing detailed anatomical images of first unfixed embryos and then living quail embryos following injection of contrast agents into the egg. So far, the earliest *in ovo* embryos we have examined have been around 7 days. We would like to use MRI to monitor effects of experimental manipulations on limb development in real time. However, operations, such as implantation of a retinoic acid bead described here, are typically being carried out in 3-day-old embryos, and the challenge will be to improve the imaging of much younger embryos. In this study, the aim was to reveal anatomy and to visualise the live embryo; no observations were made as to any detrimental effects on development which might have been caused by the contrast agent and this, too, must be examined during future studies.

We have shown the potential of MRI for imaging both normal and manipulated chick limb anatomy. The complex tissue anatomy of the chick limb was revealed by using several different MRI acquisition protocols. Separation of the different muscle groups was found to be best visualised using gradient echo protocols whereas spin echo protocols with specific T_R and T_E conditions highlighted different connective tissues. Thus, a long T_E was also found to highlight mineralised bone in the chick limb (see Fig. 4K,L), whereas a shorter T_E highlighted cartilage. Intuitively one might expect the mineralised bone to have a very short T_2 (and this is often the case, see Thompson & Chudek, 2007) but here the T_2 of the embryonic bone must be very long to give such a bright image with T_E = 40 ms. One explanation

would be that the bone at this stage is still very porous and that the water contained in these pores has a high degree of mobility.

We have demonstrated that, by using a 3D data analysis programme to merge images of the same limb acquired under different MRI conditions, the visualisation of the complex anatomy of different tissues – bone, cartilage and muscle – can be optimised. The anatomy of the duplicated chick wing showed some interesting features. For example, the detailed skeletal anatomy of the epiphyses of the forearm elements showed that the proximal epiphysis of the anterior element resembles that of the radius, whereas the distal epiphysis resembles that of an ulna. It has been well established that retinoic acid can affect not only the pattern of the digits but also the pattern of the forearm (Robson et al. 1994). Examination of the muscle pattern in the same wing also provided evidence for a duplicated forearm pattern, in that posterior muscles developed ventrally on both sides. Interestingly, in the dorsal part of the wing, the muscle pattern looked more normal. In this context, previous analysis of the effects of experimental manipulations of the chick wing also highlighted dorsoventral differences in the response to patterning signals and that skeletal and muscle patterns are not always strictly congruent with each other (Akita, 1996). The ability to visualise detailed anatomy of bone, cartilage and muscle in the same manipulated chick wing using μMRI will permit more extensive investigation of larger numbers of such manipulated limbs and will give new information about the extent to which patterning of these different tissues is co-ordinated during development.

Previous work using μMRI has shown that it is also possible to visualise the vasculature of chick embryos by injecting Gd contrast agent (Smith, 2000). It also seems likely that manganese based contrast agents could be utilised to visualise nerves (Louie, 2005). Therefore, it should be possible to work towards producing very high quality anatomical detail of all the tissues of the limb. This methodology can also be applied to other regions of the chick embryo and thus maximise the usefulness of avian embryos in the experimental analysis of development.

Acknowledgements

This work was supported by a Discipline Hopping Grant from the MRC to SC and CT, The Royal Society (XL and CT), The Anatomical Society (LM), The Wellcome Trust (SD and KS), MRC (KB and MT). The authors are deeply indebted to the late Geoff Hunter for his help and encouragement in initiating this project.

References

Akita K (1996) The effects of the ectoderm on the dorsoventral pattern of epidermis, muscles and joints in the developing chick leg: a new model. *Anat Embryol (Berl)* **193**, 377–386.

Bellairs R, Osmond M (2005) *The Atlas of Chick Development*, 2nd edn. Amsterdam: Elsevier.

Bone SN, Johnson GA, Thompson MB (1986) Three-dimensional magnetic resonance microscopy of the developing chick embryo. *Investig Radiol* **21**, 782–787.

Bruce BC, Carragher BO, Damon BM, et al. (1997) ChickScope: An interactive MRI classroom curriculum innovation for K-12. *Computers & Educ* **29**, 73–87.

Callaghan PT (1995) *Principles of Nuclear Magnetic Resonance Microscopy*. Oxford: Oxford Science Publications.

Chudek JA, Hunter G (1997) Magnetic resonance imaging in plants. In *Progress in N.M.R. Spectroscopy* (eds Emsley JW, Feeney J), Vol. 31, pp. 43–63. Oxford: Pergamon.

Davey MG, Tickle C (2007) The chicken as a model for embryonic development. *Cytogenet Genome Res* **117**, 231–239.

Dehain M, Ruffins SW, Jacob RF (2001) Three-dimensional digital movie atlas using high resolution MRI. *Dev Biol* **232**, 458–470.

Duprez D, Lapointe F, Edom-Vovard F, Kostakopoulou K, Robson L (1999) Sonic hedgehog (SHH) specifies muscle pattern at tissue and cellular level, in the chick limb bud. *Mech Dev* **82**, 151–163.

Effmann EL, Johnson GA, Smith BR, Talbott GA, Cofer G (1988) Magnetic resonance microscopy of chick embryo in ovo. *Teratology* **38**, 59–65.

Graham DL, Meier W (1975) Standards of morphological development of the quail, Cotournix coturnix japonica, embryo. *Growth* **39**, 389–400.

Hamburger V, Hamilton HL (1951) A series of normal stages in the development of the chick embryo. *J Morphol* **88**, 49–92.

Hendrick RE, Haacke EM (1993) Basic physics of MR contrast agents and maximization of image contrast. *J Magn Reson Imaging* **3**, 137–148.

Hogers B, Gross D, Lehmann V, et al. (2001) Magnetic resonance microscopy at 17.6-Tesla on chicken embryos in vitro. *J Magn Reson Imaging* **14**, 83–86.

Holder N (1978) The onset of osteogenesis in the developing chick limb. *J Embryol Exp Morphol* **44**, 15–29.

Kardon G (1998) Muscle and tendon morphogenesis in the avian hind limb. *Development* **125**, 4019–4032.

Kuhn W (1990) NMR microscopy – fundamentals, limits and possible applications. *Angew Chem Int Ed Engl* **29**, 1–12.

Louie A (2005) Magnetic resonance imaging contrast agents in the study of development. *Curr Topics* **70**, 35–56.

Nelson KL, Runge VM (1995) Basic principles of MR contrast. *Top Magn Reson Imaging* **7**, 124–136.

New DAT (1966) *The Culture of Vertebrate Embryos*, pp. 1–245. London: Logos Press.

Niswander L (2003) Pattern formation: old models out on a limb. *Nat Rev Genet* **4**, 133–143.

Robson LG, Kara T, Crawley A, Tickle C (1994) Tissue and cellular patterning of the musculature in chick wings. *Development* **120**, 1265–1276.

Ruffins SW, Martin M, Keough L, et al. (2007) Digital three-dimensional atlas of quail development using high-resolution MRI. *ScientificWorldJournal* **2**, 47–59.

Schneider JE, Bamforth SD, Farthing CR, Clarke K, Neubauer S, Bhattacharya S (2003) High-resolution imaging of normal anatomy, and neural and adrenal malformations in mouse embryos using magnetic resonance microscopy. *J Anat* **202**, 239–247.

Smith BR (2000) Magnetic resonance imaging analysis of embryos. *Methods Mol Biol* **135**, 211–216.

Smith BR, Johnson GA, Groman EV, Linney E (1994) Magnetic resonance microscopy of mouse embryos. *Dev Biol* **91**, 3530–3533.

Thompson TJU, Chudek JA (2007) A novel approach to the visualisation of heat-induced structural change in bone. *Science and Justice* **47**, 99–104.

Tickle C (2004) The contribution of chicken embryology to the understanding of vertebrate limb development. *Mech Dev* **121**, 1019–1029.

Tickle C, Lee J, Eichele G (1985) A quantitative analysis of the effect of all-trans-retinoic acid on the pattern of chick development. *Dev Biol* **109**, 82–95.

Supplementary material

The following supplementary material is available for this article:

Video Clip S1. μMRI spin echo images of chick embryos. (a) Longitudinal slices from a 3D dataset with T_R/T_E = 200/6.3 ms. (b) 3D surface rendering from that dataset showing anatomy manually extracted using AMIRA. Matrix size is $128 \times 128 \times 128$. Field of view and voxel dimensions, $10 \times 10 \times 10$ mm; $80 \times 80 \times 80$ μm.

Video Clip S2. 3D μMRI spin echo images of chick embryos. (a–b) Full datasets showing slices through a Day 6 embryo (Gd contrast agent applied *in vivo*, fixed after 1 h and embedded in agar containing contrast agent), T_R/T_E = 300/10 ms, Matrix size: $512 \times 512 \times 512$. Field of view and voxel dimensions, $10.0 \times 10.0 \times 10.0$ mm; $20 \times 20 \times 20$ μm.

Video Clip S3. 3D μMRI spin echo image of a live Day 7 quail embryo in its egg, after injection with contrast agent in the brain showing regions of interest surface rendered using AMIRA software. Matrix size is $128 \times 128 \times 128$. Field of view and voxel dimensions, $30.0 \times 30.0 \times 30.0$ mm; $240 \times 240 \times 240$ μm.

Video Clip S4. (a and b) 3D AMIRA reconstructions of μMRI spin echo images of excised Day 10 and Day 14 chick embryo wings.

Video Clip S5. μMRI gradient-echo images of chick embryo leg showing 3D surface rendering of bones and individual muscles using AMIRA software. T_R/T_E = 1000/40 ms. Matrix size is $128 \times 128 \times 128$. Field of view and voxel dimensions, $25.0 \times 25.0 \times 25.0$ mm; $200 \times 200 \times 200$ μm.

Video Clip S6. μMRI images of a Day 13, 43234 experimentally manipulated chick wing. (a) Data from spin echo acquisition, T_R/T_E = 300/40 ms and (b) animation of surface rendering of data. Matrix size is $256 \times 256 \times 256$. Field of view and voxel dimensions, $12.0 \times 12.0 \times 12.0$ mm; $50 \times 50 \times 50$ μm.

This material is available as part of the online article from: http://www.blackwell-synergy.com/doi/abs/DOI:10.1111/j.1469-7580.2007.00825.x (This link will take you to the article abstract).

Please note: Blackwell Publishing are not responsible for the content or functionality of any supplementary materials supplied by the authors. Any queries (other than missing material) should be directed to the corresponding author for the article.